Available online at www.sciencedirect.com
SCIENCE DIRECT
Journal of Sound and Vibration 295 (2006) 1076–1084
JOURNAL OF SOUND AND VIBRATION
www.elsevier.com/locate/jsvi

Short Communication

High frequency energy characterization of beam structures based only on driving point mobility or impedance

Seungbo Kim, Rajendra Singh*

Acoustics and Dynamics Laboratory, Department of Mechanical Engineering, The Center for Automotive Research, The Ohio State University, Suite 255, 650 Ackerman Road, Columbus, Ohio 43202, USA

Received 1 September 2005; received in revised form 1 September 2005; accepted 16 October 2005
Available online 12 May 2006

Abstract

This article describes a characterization method to specifically determine the asymptotic behavior of kinetic and potential energies at higher frequencies with the driving point measures only. Longitudinal and flexural motions of semi-infinite and finite beam structures are considered when a harmonic force excitation is applied. Our method predicts spectral energies well at high frequencies unlike the existing methods that are limited to low frequencies and/or lightly damped case. The new method is insensitive to the driving point mobility or impedance formulations and yields consistent results.

1. Introduction

Recently, we proposed a method that characterizes the spectral kinetic or potential energy input to structures by driving point mobility or impedance only [1]. This method in our earlier paper overcomes some deficiencies of the existing methods [2,3]. However, such spectral characterization methods are still limited to lower frequencies and/or lightly damped system since the estimates deviate significantly as the frequency or damping loss factor increases [1–3]. In this communication, we extend the methods [1–3] to higher frequencies with application to semi-infinite and finite beams.

Energy-based methods are widely used in vibro-acoustic modeling [4–10]. Some methods are statistical in nature, and thus are more suitable at high frequencies, especially when the high modal density assumption is ensured [4–7]. Deterministic energy methods have also been employed in vibration transmission, isolation and transfer path analyses over a wide range of frequencies [7–10]. Typically, the driving point information at the sub-system interfaces represents the sub-system behavior in such modeling techniques and most of the energy-based methods are based on the dissipated energy (power) concept [4–10]. However, the kinetic or potential energy input may be more suitable for describing the vibrational behavior of sub-systems than the dissipated energy (power) level. For instance, our earlier article clearly shows that the dissipated energy may not exhibit much reduction by the application of high damping although the kinetic energy input is significantly diminished at higher frequencies [1]. Nonetheless, lack of an appropriate spectral kinetic or potential energy

*Corresponding author. Tel.: +1 614 292 9044; fax: +1 614 292 3163.
E-mail address: singh.3@osu.edu (R. Singh).

0022-460X/$ - see front matter
doi:10.1016/j.jsv.2005.10.027

calculation method at higher frequencies hinders proper understanding of vibro-acoustic behavior. This communication attempts to partially remedy this by suggesting a method that would characterize the kinetic and potential energies at high frequencies with only driving point transfer function information. The scope is limited to a linear time-invariant system, and longitudinal and flexural motions of semi-infinite and finite beam structures are analyzed in the frequency domain given a single harmonic force excitation. Chief objectives of our study are: (1) examine the asymptotic behavior of energy characteristics at higher frequencies; (2) clarify the role of structural damping; (3) propose a method (designated here as Method 4, as a continuation of three methods described in Ref. [1]) to estimate the spectral energies at high frequencies via the driving point transfer mobility or impedance.

2. Asymptotic energy behavior of a semi-infinite beam at high frequencies

A semi-infinite beam of Fig. 1 is considered to analyze the asymptotic energy behavior at high frequencies. A harmonic force excitation at frequency ω is applied to the beam in axial or transverse directions separately to examine the longitudinal or flexural motions.

Harmonic velocity (v), displacement (ξ) and its gradient in longitudinal motions of the semi-infinite beam given a force of amplitude f_0 at ω are written as follows where ρ and S are the mass density and the cross-sectional area, respectively:

$$v(x) = \mathrm{j}\omega\xi(x) = \frac{f_0}{S\sqrt{\rho\widetilde{\mathrm{E}}}}\exp(-\widetilde{\kappa}_L x\mathrm{j}), \quad \frac{\partial\xi(x)}{\partial x} = -\frac{f_0}{S\widetilde{\mathrm{E}}}\exp(-\widetilde{\kappa}_L x\mathrm{j}). \tag{1,2}$$

Here, η is the damping loss factor, and $\widetilde{\mathrm{E}}$, and $\widetilde{\kappa}_L$ represent the complex modulus and the longitudinal wavenumber, respectively, and are expressed as follows where superscripts $'$ and $''$ denote the real and imaginary parts, respectively:

$$\widetilde{\mathrm{E}}(\omega) = \mathrm{E}'(1+\mathrm{j}\eta) = \mathrm{E}' + \mathrm{j}\mathrm{E}'', \quad \widetilde{\kappa}_L = \omega\sqrt{\rho/\widetilde{\mathrm{E}}} = \kappa_L' + \mathrm{j}\kappa_L'' \approx \omega\sqrt{\rho/\mathrm{E}'}[(1-\mathrm{j}\eta/2)]. \tag{3,4}$$

Spectral kinetic, potential and dissipated energies within the semi-infinite beam are derived as follows where $\overline{E}_m$, $\overline{E}_k$ and $\overline{E}_d$ represent the time-averaged kinetic, potential and dissipated energies, respectively, at frequency ω and the superscript * denotes the complex conjugate:

$$\begin{aligned}\overline{E}_m(\omega) &= \frac{\rho S}{2}\int_0^\infty |v(x)|^2\,\mathrm{d}x = \frac{\rho S}{2}\int_0^\infty v(x)\cdot v^*(x)\,\mathrm{d}x \\ &= \frac{\rho S}{2}\int_0^\infty \frac{|f_0|^2}{\rho S^2|\widetilde{\mathrm{E}}|}\exp\left(2\kappa_L'' x\right)\mathrm{d}x = \frac{-|f_0|^2}{4S|\widetilde{\mathrm{E}}|\kappa_L''},\end{aligned} \tag{5}$$

$$\begin{aligned}\overline{E}_k(\omega) &= \frac{S\mathrm{E}'}{2}\int_0^\infty \left|\frac{\partial\xi(x)}{\partial x}\right|^2\mathrm{d}x = \frac{S\mathrm{E}'}{2}\int_0^\infty \frac{\partial\xi(x)}{\partial x}\cdot\left[\frac{\partial\xi(x)}{\partial x}\right]^*\mathrm{d}x \\ &= \frac{S\mathrm{E}'}{2}\int_0^\infty \frac{|f_0|^2}{S^2|\widetilde{\mathrm{E}}|^2}\exp\left(2\kappa_L'' x\right)\mathrm{d}x = \frac{-\mathrm{E}'|f_0|^2}{4S|\widetilde{\mathrm{E}}|\kappa_L''},\end{aligned} \tag{6}$$

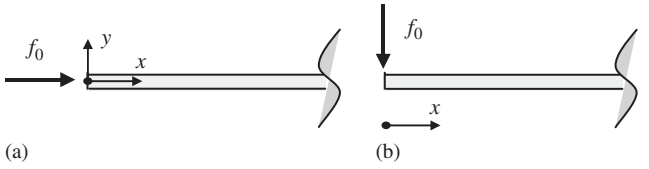

Fig. 1. Semi-infinite beam given a sinusoidal force excitation at the free edge ($x = 0$): (a) Under longitudinal excitation; (b) under transverse excitation.

$$\overline{E}_d(\omega)\frac{S\mathrm{E}''}{2}\int_0^\infty \left|\frac{\partial\xi(x)}{\partial x}\right|^2 \mathrm{d}x = \frac{-\mathrm{E}''|f_0|^2}{4S|\widetilde{\mathrm{E}}|\kappa_L''}. \tag{7}$$

Note that κ_L'' is a negative value for positive damping loss factors as shown in Eq. (4), and the integrations of Eqs. (5–7) converge to a finite value.

Next, the flexural motions of the semi-infinite beam of Fig. 1(b) are considered. The flexural velocity field at ω is

$$v(x) = \frac{\omega f_0}{\widetilde{\mathrm{E}}\mathrm{I}\widetilde{\kappa}_B^3(1+\mathrm{j})}\begin{bmatrix}\exp(-\widetilde{\kappa}_B x\mathrm{j}) \\ +\exp(-\widetilde{\kappa}_B x)\end{bmatrix}, \quad v^*(x) = \frac{\omega f_0}{\widetilde{\mathrm{E}}^*\mathrm{I}\widetilde{\kappa}_B^{*3}(1-\mathrm{j})}\begin{bmatrix}\exp(\widetilde{\kappa}_B^* x\mathrm{j}) \\ +\exp(-\widetilde{\kappa}_B^* x)\end{bmatrix}. \tag{8,9}$$

Here, I is the area moment of inertia and the following $\tilde{\kappa}_B$ represent the complex flexural wave number where superscripts $'$ and $''$ denote the real and imaginary parts, respectively:

$$\widetilde{\kappa}_B = \sqrt[4]{\omega^2\rho S/\widetilde{\mathrm{E}}\mathrm{I}} = \kappa_B' + \mathrm{j}\kappa_B'' \approx \sqrt[4]{\omega^2\rho S/\mathrm{I}\mathrm{E}'}[(1-\mathrm{j}\eta/4)]. \tag{10}$$

Then, time-averaged kinetic energy within the semi-infinite beam is derived as follows by integrating the squared-magnitude of velocity:

$$|v(x;\omega)|^2 = v(x)\cdot v^*(x) = \frac{\omega^2|f_0|^2}{2|\widetilde{\mathrm{E}}|^2\mathrm{I}^2|\kappa_B|^6}\begin{bmatrix}\exp(2\kappa_B'' x)+\exp(-2\kappa_B' x) \\ +2\exp(-\kappa_B' x+\kappa_B'' x)\cdot\cos(-\kappa_B' x+\kappa_B'' x)\end{bmatrix}, \tag{11}$$

$$\overline{E}_m(\omega) = \frac{\rho S}{2}\int_0^\infty |v(x)|^2\,\mathrm{d}x = \frac{|f_0|^2}{4|\widetilde{\mathrm{E}}|\mathrm{I}|\kappa_B|^2}\left[\frac{\kappa_B''-\kappa_B'}{2\kappa_B'\kappa_B''}+\frac{1}{\kappa_B'-\kappa_B''}\right]. \tag{12}$$

Similarly, time-averaged potential and dissipated energies within the semi-infinite beam are obtained as follows by using the squared-magnitude of $\partial^2\xi(x)/\partial x^2$:

$$\xi(x) = \frac{f_0}{\widetilde{\mathrm{E}}\mathrm{I}\widetilde{\kappa}_B^3(\mathrm{j}-1)}\begin{bmatrix}\exp(-\widetilde{\kappa}_B x\mathrm{j}) \\ +\exp(-\widetilde{\kappa}_B x)\end{bmatrix}, \quad \frac{\partial^2\xi(x)}{\partial x^2} = \frac{f_0}{\widetilde{\mathrm{E}}\mathrm{I}\widetilde{\kappa}_B(1-\mathrm{j})}\begin{bmatrix}\exp(\widetilde{\kappa}_B^* x\mathrm{j}) \\ -\exp(-\widetilde{\kappa}_B^* x)\end{bmatrix}, \tag{13,14}$$

$$\begin{aligned}\left|\frac{\partial^2\xi(x)}{\partial x^2}\right|^2 &= \frac{\partial^2\xi(x)}{\partial x^2}\cdot\left[\frac{\partial^2\xi(x)}{\partial x^2}\right]^* \\ &= \frac{|f_0|^2}{2|\widetilde{\mathrm{E}}|^2\mathrm{I}^2|\kappa_B|^2}\begin{bmatrix}\exp(2\kappa_B'' x)+\exp(-2\kappa_B' x) \\ -2\exp(-\kappa_B' x+\kappa_B'' x)\cdot\cos(-\kappa_B' x+\kappa_B'' x)\end{bmatrix},\end{aligned} \tag{15}$$

$$\overline{E}_k(\omega) = \frac{\mathrm{E}'\mathrm{I}}{2}\int_0^\infty \left|\frac{\partial^2\xi(x)}{\partial x^2}\right|^2 \mathrm{d}x = \frac{\mathrm{E}'|f_0|^2}{8|\widetilde{\mathrm{E}}|^2\mathrm{I}}\left[\frac{1}{\kappa_B'\kappa_B''(\kappa_B''-\kappa_B')}\right], \tag{16}$$

$$\overline{E}_d(\omega) = \frac{\mathrm{E}''\mathrm{I}}{2}\int_0^\infty \left|\frac{\partial^2\xi(x)}{\partial x^2}\right|^2 \mathrm{d}x = \frac{\mathrm{E}''|f_0|^2}{8|\widetilde{\mathrm{E}}|^2\mathrm{I}}\left[\frac{1}{\kappa_B'\kappa_B''(\kappa_B''-\kappa_B')}\right]. \tag{17}$$

Similar to the longitudinal motion case, κ_B'' of Eq. (10) is a negative value for positive damping loss factors, and the integrations of Eqs. (12,16,17) converge to a finite value.

3. Effect of damping of the energy behavior of a semi-infinite beam

The spectral energy levels, $\overline{E}_m$, $\overline{E}_k$ and $\overline{E}_d$ for both longitudinal and flexural motions, are shown in Figs. 2(a,b) and (c,d). Observe that $\overline{E}_m$ and $\overline{E}_k$ match each other but the discrepancy between them is relatively higher in flexural motion with high damping ($\eta = 0.2$). Further, Fig. 2 shows that $\overline{E}_d$ remains the same for low ($\eta = 0.08$) and high ($\eta = 0.2$) damping cases while $\overline{E}_m$ or $\overline{E}_k$ decreases as the damping increases for

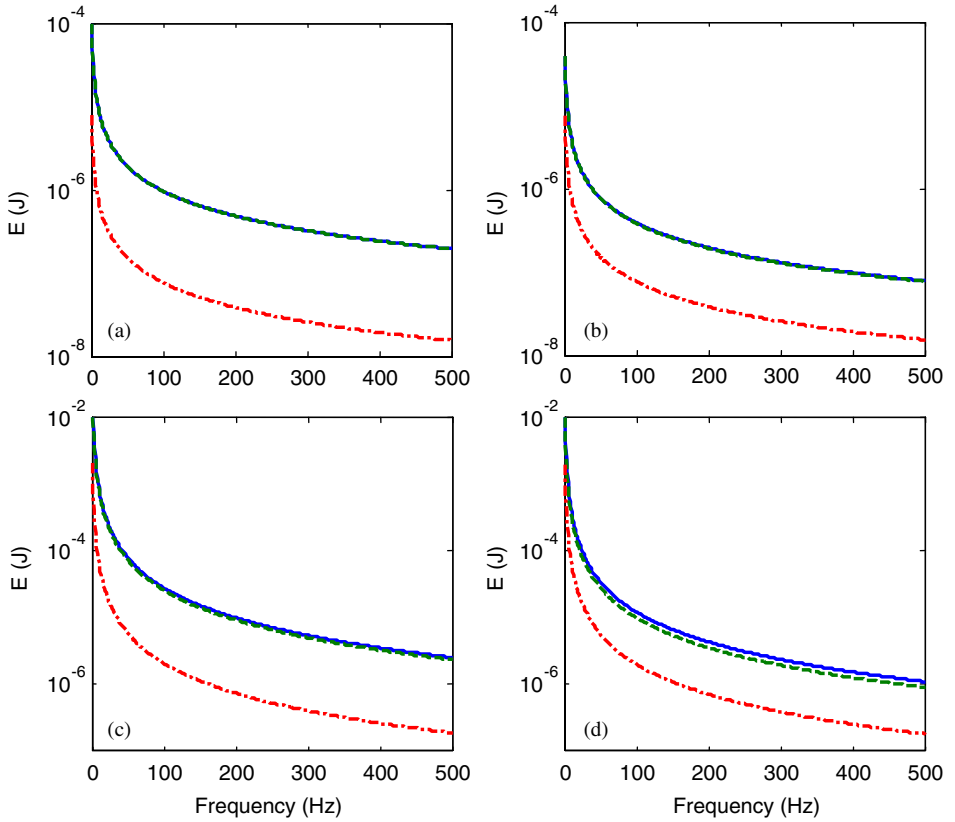

Fig. 2. Spectral energies for a semi-infinite beam of Fig. 1 given a force excitation at the free end: (a) Longitudinal motion of a lightly damped system ($\eta = 0.08$); (b) longitudinal motion of a heavily damped system ($\eta = 0.2$); (c) flexural motion of a lightly damped system ($\eta = 0.08$); (d) flexural motion of a heavily damped system ($\eta = 0.2$). Key: ——, Kinetic energy; – – – –, potential energy; — · — ·, dissipated energy.

longitudinal or flexural motions. This observation is consistent with the result that was reported in our earlier article [1].

4. Development of a new energy characterization method

The driving point mobility (M_{L0}) and impedance (Z_{L0}) of the semi-infinite beam in longitudinal motions are written as follows where subscript L implies axial motions:

$$M_{L0}(\omega) = \frac{1}{S\sqrt{\rho\tilde{\mathrm{E}}}} \approx \frac{1}{S\sqrt{\rho \mathrm{E}'}}\left[\left(1 - \mathrm{j}\frac{\eta}{2}\right)\right], \tag{18}$$

$$Z_{L0}(\omega) = S\sqrt{\rho\tilde{\mathrm{E}}} \approx S\sqrt{\rho \mathrm{E}'}\left[\left(1 + \mathrm{j}\frac{\eta}{2}\right)\right]. \tag{19}$$

By using M_{L0} and Z_{L0}, the damping loss factor can be estimated as follows where Re and Im represent the real and imaginary parts of a complex quantity respectively and the superscript $\hat{}$ denotes the estimate:

$$\hat{\eta} = 2\left|\frac{\mathrm{Im}(M_{L0})}{\mathrm{Re}(M_{L0})}\right| = 2\left|\frac{\mathrm{Im}(Z_{L0})}{\mathrm{Re}(Z_{L0})}\right|. \tag{20}$$

The driving point mobility (M_{B0}) and impedance (Z_{B0}) of the semi-infinite beam in flexural motions are expressed as follows where subscript B denotes the transverse motions:

$$M_{B0}(\omega)=\frac{2\omega}{\widetilde{\mathrm{E}}\mathrm{I}\widetilde{\kappa}_B^3(1+\mathrm{j})}\approx\frac{1}{\sqrt[4]{\mathrm{I}\mathrm{E}'\omega^2(\rho S)^3}}\left[\left(1-\frac{\eta}{4}\right)-\mathrm{j}\left(1+\frac{\eta}{4}\right)\right], \tag{21}$$

$$Z_{B0}(\omega)=\frac{\widetilde{\mathrm{E}}\mathrm{I}\widetilde{\kappa}_B^3(1+\mathrm{j})}{2\omega}\approx\frac{\sqrt[4]{\mathrm{I}\mathrm{E}'\omega^2(\rho S)^3}}{2}\left[\left(1-\frac{\eta}{4}\right)+\mathrm{j}\left(1+\frac{\eta}{4}\right)\right]. \tag{22}$$

Similar to the longitudinal motions, the damping loss factor is estimated as follows by using M_{B0} and Z_{B0}:

$$\widehat{\eta}=2\left[\left|\frac{\mathrm{Im}(M_{B0})}{\mathrm{Re}(M_{B0})}\right|-1\right]=2\left[\left|\frac{\mathrm{Im}(Z_{B0})}{\mathrm{Re}(Z_{B0})}\right|-1\right]=\frac{\eta}{1-\eta/4}. \tag{23}$$

By using the estimated damping loss factor, time-averaged kinetic and potential energies are approximated at higher frequencies as follows where $\overline{E}$ is the estimate of time-averaged energy:

$$\overline{E}_m\approx\overline{E}_k\approx\widehat{\overline{E}}_{4,m}=\widehat{\overline{E}}_{4,k}=\overline{E}_d/\widehat{\eta}. \tag{24}$$

Here, estimation (24) at high frequencies is designated as Method 4 and is denoted by subscript 4; refer to Method 1, 2 or 3 in Ref. [1]. Further, note that the assumption made here, $\overline{E}_m\approx\overline{E}_k$, is generally valid at higher frequencies as observed in Fig. 2; it has been suggested by many researchers [4,7]. Further, since the damping estimation formulation (23) for flexural motions differs from the one (20) for longitudinal motions, Method 4 must be separately applied to longitudinal or flexural motions.

The energy estimates for the semi-infinite beam are calculated to examine the high frequency behavior. Results are shown in Figs. 3(a,b) and (c,d) for longitudinal and flexural motions, respectively. Method 4 is also compared in Fig. 3 with the energy estimates that have been proposed earlier by us (Method 3 in Ref. [1]) and other researchers (Method 2 in Ref. [3]). Note that Method 2 predicts the following energies where subscripts 1, 2, M and Z indicate estimates using Methods 1, 2, mobility and impedance, respectively:

$$\left[\widehat{\overline{E}}_{2Z,m}(\omega)+\widehat{\overline{E}}_{2Z,k}(\omega)\right]=\left[\widehat{\overline{E}}_{1Z,m}(\omega)+\widehat{\overline{E}}_{1Z,k}(\omega)\right]/\alpha_Z(\omega), \tag{25}$$

$$\left[\widehat{\overline{E}}_{2M,m}(\omega)+\widehat{\overline{E}}_{2M,k}(\omega)\right]=\left[\widehat{\overline{E}}_{1M,m}(\omega)+\widehat{\overline{E}}_{1M,k}(\omega)\right]/\alpha_M(\omega), \tag{26}$$

$$\widehat{\overline{E}}_{1Z,m}=\mathbf{V}_D^{*\mathrm{T}}\,\mathrm{Im}\left[\mathbf{Z}_D/\omega+\partial\mathbf{Z}_D/\partial\omega\right]\mathbf{V}_D/4, \tag{27}$$

$$\widehat{\overline{E}}_{1Z,k}=-\mathbf{V}_D^{*\mathrm{T}}\,\mathrm{Im}\left[\mathbf{Z}_D/\omega-\partial\mathbf{Z}_D/\partial\omega\right]\mathbf{V}_D/4, \tag{28}$$

$$\widehat{\overline{E}}_{1M,m}=\mathbf{F}_D^{*\mathrm{T}}\,\mathrm{Im}\left[\mathbf{M}_D/\omega+\partial\mathbf{M}_D/\partial\omega\right]\mathbf{F}_D/4, \tag{29}$$

$$\widehat{\overline{E}}_{1M,k}=-\mathbf{F}_D^{*\mathrm{T}}\,\mathrm{Im}\left[\mathbf{M}_D/\omega-\partial\mathbf{M}_D/\partial\omega\right]\mathbf{F}_D/4. \tag{30}$$

Here, $\mathbf{Z}$ and $\mathbf{M}$ are the impedance and mobility matrices, and $\mathbf{F}$ and $\mathbf{V}$ are the force and velocity amplitude vectors respectively. Further, the subscript D and the superscript T imply the driving point and the matrix transpose, respectively. Further, α_Z and α_M are the correction factors for impedance and mobility, respectively, that have been introduced in Method 2. Refer to the literature for further details of Methods 1 [2] or 2 [3].

The energy estimates from Method 3, denoted by subscript 3, are summarized as

$$\widehat{\overline{E}}_{3Z,m}=|\widetilde{E}_{Z,m}|,\quad \widehat{\overline{E}}_{3Z,k}=|\widetilde{E}_{Z,k}|, \tag{31,32}$$

$$\widetilde{E}_{Z,m}=\frac{1}{4\mathrm{j}}v_1\left[\frac{z_{\mathrm{D}11}}{\omega}+\frac{\partial z_{\mathrm{D}11}}{\partial\omega}\right]v_1,\quad \widetilde{E}_{Z,k}\approx\frac{1}{4\mathrm{j}}v_1\left[\frac{z_{\mathrm{D}11}}{\omega}-\frac{\partial z_{\mathrm{D}11}}{\partial\omega}\right]v_1. \tag{33,34}$$

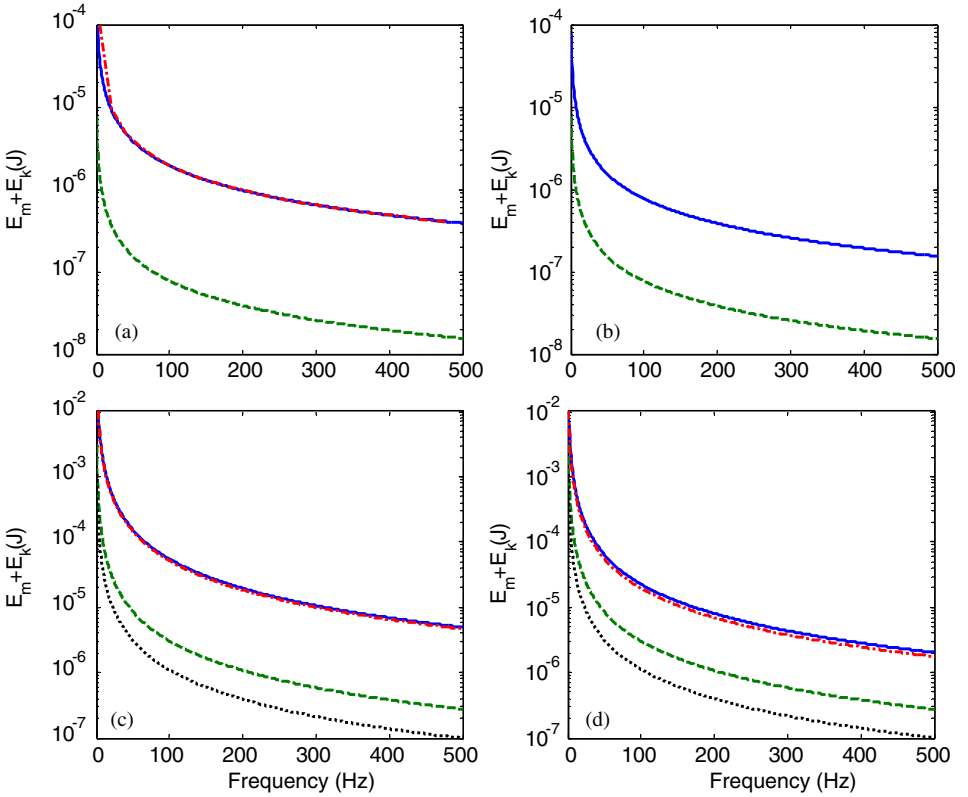

Fig. 3. Sum of time-averaged kinetic and potential energies of a semi-infinite beam of Fig. 1 given a force excitation at the free end: (a) Lightly damped system ($\eta = 0.08$) in longitudinal motion; (b) heavily damped system ($\eta = 0.2$) in longitudinal motion; (c) Lightly damped system ($\eta = 0.08$) in flexural motion; (d) heavily damped system ($\eta = 0.2$) in flexural motion. Key: ——, Exact; — · — ·, Method 4; – – – –, Method 3; ·····, Method 2. Here, the lines —— and — · — · almost overlap in (a)–(c).

Here, $\widetilde{E}_m$ and $\widetilde{E}_k$ are the complex-valued spectral kinetic and potential energies respectively. Refer to Ref. [1] for further details of Method 3. Figs. 3(a,b) shows that the estimates of $\overline{E}_m + \overline{E}_k$ from Method 4 perfectly match the exact values in longitudinal motions. But a small deviation in $\widehat{\overline{E}}_{4m} + \widehat{\overline{E}}_{4k}$ from the exact one value is observed for the high damping case in flexural motions, as shown in Fig. 3(d). Further, the estimates with Method 2 or 3 deviate significantly from the exact energy in both longitudinal and flexural motions and the deviations of $\widehat{\overline{E}}_{2m} + \widehat{\overline{E}}_{2k}$ are larger than the ones of $\widehat{\overline{E}}_{3m} + \widehat{\overline{E}}_{3k}$, as shown in Fig. 3. Nonetheless, both $\widehat{\overline{E}}_{2m} + \widehat{\overline{E}}_{2k}$ and $\widehat{\overline{E}}_{3m} + \widehat{\overline{E}}_{3k}$ produce consistent results with mobility or impedance for the semi-infinite beam case. Further note that $\widehat{\overline{E}}_{2m} + \widehat{\overline{E}}_{2k}$ in longitudinal motion is zero and is not shown in Figs. 3(a,b) since the longitudinal mobility and impedance of Eqs. (18,19) are constant with frequency and their derivatives (which represent $\widehat{\overline{E}}_{2m} + \widehat{\overline{E}}_{2k}$) are zero.

5. High frequency energy behavior of a finite beam

Like the semi-infinite beam case, a finite beam of Fig. 4 (with clamped–free boundaries) is examined next at higher frequencies. Longitudinal and flexural motions are separately considered by applying a harmonic force (of amplitude f_0) to the free end (at $x = 0$) in the corresponding directions, as shown in Figs. 4(a) and (b), respectively. Time-averaged kinetic, potential and dissipated energy inputs to the clamped–free beam in longitudinal and flexural motions have been formulated in Ref. [1], thus, refer to that paper for details.

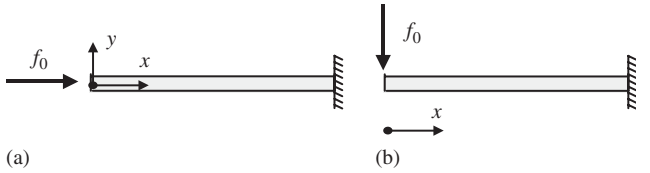

Fig. 4. Finite beam given a sinusoidal force excitation at the free edge: (a) Under longitudinal excitation; (b) under transverse excitation.

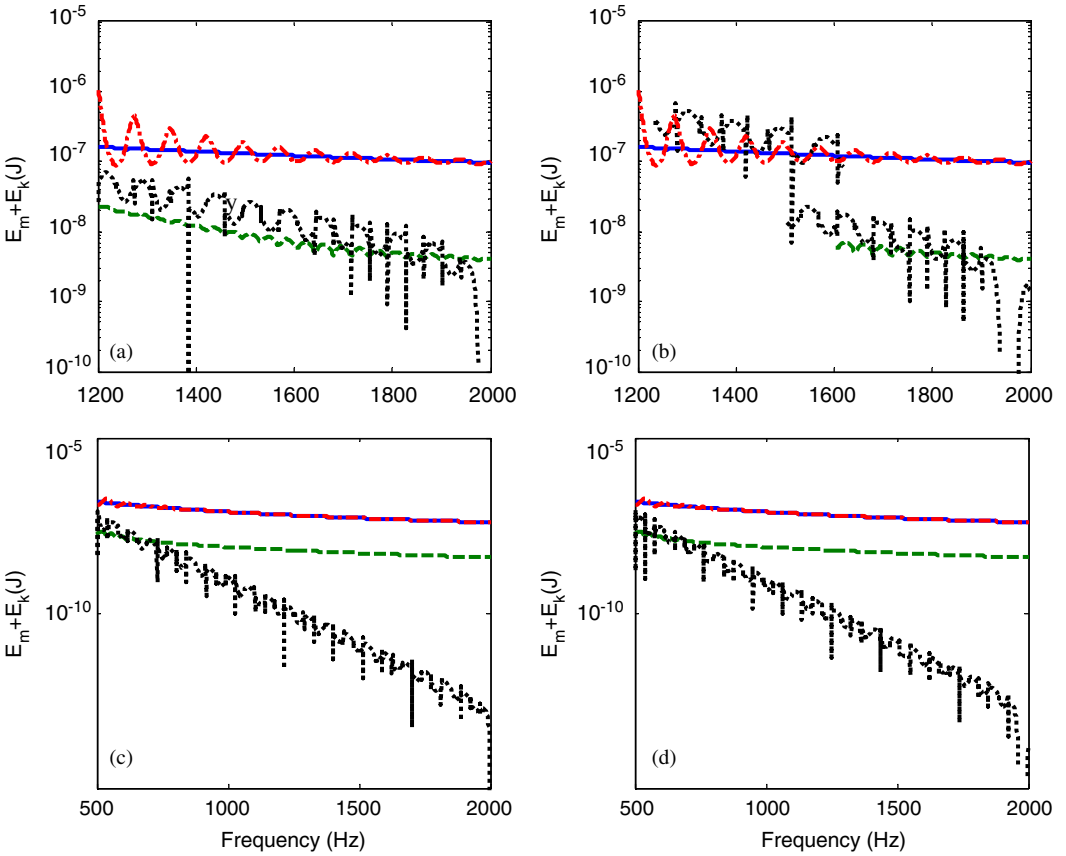

Fig. 5. Sum of time-averaged kinetic and potential energies for longitudinal motions of a finite beam of Fig. 4(a) given a force excitation at the free end: (a) Lightly damped system ($\eta = 0.08$) with impedance; (b) lightly damped system ($\eta = 0.08$) with mobility; (c) heavily damped system ($\eta = 0.2$) with impedance; (d) heavily damped system ($\eta = 0.2$) with mobility. Key: ——, Exact; — · — ·, Method 4; - - - -, Method 3; ·····, Method 2. Here, the lines —— and — · — · almost overlap in (c) and (d).

The energy estimates and exact values are shown in Fig. 5 for longitudinal motions. The estimates of $\overline{E}_m + \overline{E}_k$ from Method 4 asymptotically approach the exact values and two curves become almost identical as the frequency increases. Like the semi-infinite beam case, the estimates with both Methods 2 and 3 deviate significantly from the exact energy. Fig. 5 shows that the $\widehat{\overline{E}}_{2m} + \widehat{\overline{E}}_{2k}$ rapidly decrease as the frequency increases and this asymptotic behavior of $\widehat{\overline{E}}_{2m} + \widehat{\overline{E}}_{2k}$ is different from the exact ones, unlike the semi-infinite beam. It is expected that $\widehat{\overline{E}}_{2m} + \widehat{\overline{E}}_{2k}$ will approach zero, which represents the ideal asymptotic behavior of the semi-infinite structure, as the frequency is increased further.

Flexural motions of the finite beam of Fig. 4(b) are also examined and calculated results are shown in Fig. 6. Like the longitudinal motion case, Fig. 6 shows that predictions of Method 4 match well with the exact $\overline{E}_m + \overline{E}_k$ at higher frequencies. Similar to the semi-infinite beam case, both $\widehat{\overline{E}}_{2m} + \widehat{\overline{E}}_{2k}$ and $\widehat{\overline{E}}_{3m} + \widehat{\overline{E}}_{3k}$

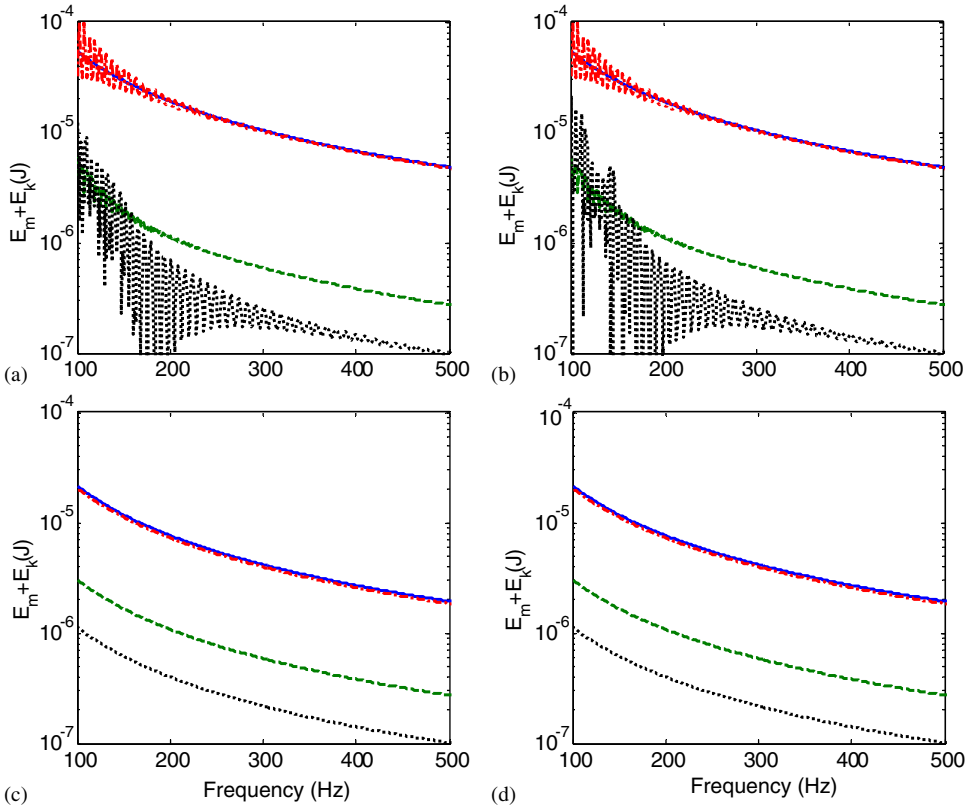

Fig. 6. Sum of time-averaged kinetic and potential energies for flexural motions of a finite beam of Fig. 4(b) given a force excitation at the free end: (a) Lightly damped system ($\eta = 0.08$) with impedance; (b) lightly damped system ($\eta = 0.08$) with mobility; (c) heavily damped system ($\eta = 0.2$) with impedance; (d) heavily damped system ($\eta = 0.2$) with mobility. Key: ——, Exact; — · — ·, Method 4; - - - -, Method 3; ·····, Method 2. Here, the lines —— and — · — · almost overlap in (c) and (d).

significantly differ from $\overline{E}_m + \overline{E}_k$ but the deviation is larger for $\widehat{\overline{E}}_{2m} + \widehat{\overline{E}}_{2k}$ than the one for $\widehat{\overline{E}}_{3m} + \widehat{\overline{E}}_{3k}$, as seen in Fig. 6. In both longitudinal and flexural motions, Methods 3 and 4 yield the most consistent predictions with mobility or impedance formulations at all frequencies, as shown in Figs. 5 and 6. Method 2 also predicts the same asymptotic behavior with mobility or impedance at higher frequencies but some differences are observed between the estimations in the resonance regions of Figs. 5 and 6. Note that negative values are not displayed in logarithmic plots of Figs. 5 and 6, and thus the lines with the negative values for energy estimates are discontinuous at some frequencies.

6. Conclusion

Energy characteristics over the high frequency regime have been examined, with applications to longitudinal and flexural motions of semi-infinite and finite beam structures. Kinetic and potential energies match well but discrepancy between them is relatively higher in flexural motion with high damping. Further, the dissipated energy remains the same for low ($\eta = 0.08$) and high ($\eta = 0.2$) damping cases while the kinetic or potential energy decreases as the damping is increased in longitudinal or flexural motions. The aforementioned observation is consistent with the finite beam case that was reported in our earlier article [1]. A method has been suggested to characterize the spectral energy of a beam structure over the high frequency regime. Our energy estimates are very close to exact values. Like the low frequency method that was reported earlier [1], our method is insensitive to the driving point mobility or impedance formulations and yields consistent results. Finally, our method does not require a prior knowledge of the transfer functions.

Further work is required to extend our methodology to complex structures at high frequencies and to improve the energy characterization schemes over the middle frequency regime. Moreover, a method that could quantify paths or sources needs to be developed along with the energy characterization scheme especially when multiple inputs are applied to a vibratory system.

Acknowledgment

The Center for Automotive Research Industrial Consortium (Noise, Vibration and Dynamics Thrust) at The Ohio State University is gratefully acknowledged for supporting this research.

References

[1] S. Kim, R. Singh, Alternate methods for characterizing spectral energy inputs based only on driving point mobilities or impedances, *Journal of Sound and Vibration* 291 (3–5) (2006) 604–626.
[2] Y.I. Bobrovnitskii, Estimating the vibrational energy characteristics of an elastic structure via the input impedance and mobility, *Journal of Sound and Vibration* 217 (2) (1998) 351–386.
[3] Y.I. Bobrovnitskii, M.P. Korotkov, Improved estimates for the energy characteristics of a vibrating elastic structure via the input impedance and mobility: experimental verification, *Journal of Sound and Vibration* 247 (4) (2001) 683–702.
[4] R.H. Lyon, R.G. Dejong, *Theory and Application of Statistical Energy Analysis*, Butterworth-Heinemann, Boston, 1995.
[5] J.L. Wohlever, R.J. Bernhard, Mechanical energy flow models of rods and beams, *Journal of Sound and Vibration* 153 (1) (1992) 1–19.
[6] G. Orefice, C. Cacciolati, J.L. Guyader, The energy mobility, *Journal of Sound and Vibration* 254 (2) (2002) 269–295.
[7] L. Cremer, M. Heckle, *Structure-Borne Sound: Structural Vibrations and Sound Radiation at Audio Frequencies*, Springer, New York, 1973.
[8] S. Kim, R. Singh, Vibration transmission through an isolator modeled by continuous system theory, *Journal of Sound and Vibration* 248 (5) (2001) 925–953.
[9] T.E. Rook, R. Singh, Mobility analysis of structure-borne noise power flow through bearings in gearbox-like structures, *Noise Control Engineering Journal* 44 (2) (1996) 69–78.
[10] R. Singh, S. Kim, Examination of multi-dimensional vibration isolation measures and their correlation to sound radiation over a broad frequency range, *Journal of Sound and Vibration* 262 (3) (2003) 419–455.